An Assessment of Particle Production Hazard as a Function of Fault Time, Line Amperage, Conductor Configuration, and Conductor Type

Brendan P. Dooher (Wyvernn), Scott Hayes (PG&E)
Brendan.dooher@wyvernn.com
scott.hayes@pge.com

1 INTRODUCTION

The purpose of the project was to determine the relationship between the interrupt time, line current, and fault type and the particles released during a fault, and the resultant fire ignition hazard. This testing was performed at the ATS High Current Test Yard in San Ramon, CA from October 2 to October 15, 2019. This portion of the analysis was conducted using a FLIR high speed thermal imaging camera that takes thermal videos of the fault and resulting particle blast and fallout. This document is a technical summary showing the results of the FLIR A8303sc infrared imaging of flashover events resulting from phase to phase contact between two different conductors of various configurations and attempts to place some of the data into an initial framework.

Phase-to-phase overhead fault testing was conducted at three fault current magnitudes, (1000 amps, 4000 amps, and 7000 amps) using three different conductor types (#4 ACSR, 397 MCM Al and 3/0 CU) at various fault clearing times ranging from 0.1s to 1.5s. Tests were conducted in two different environments; one was the high current yard “Cage” where the test conductors were at approximately 10 feet in height. These tests occurred for all current magnitudes. The second phase of the test occurred in the open yard using the “Lift”, with heights initially at 15’ to finally being conducted at 40’, using both a standardized Cal-Fire approved fuel bed (dried grass) and 40 lb white virgin kraft paper. In addition to standard conductors, phase-to-ground fault testing was conducted between the conductor and a grounded section of structural steel angle iron to simulate a conductor-to-tower contact scenario. All testing was performed at 21kV line-to-line voltage, the maximum voltage available in the test yard.

There are a few major independent variables for these tests. Primary among these variables is interrupt fault time. Conductor configurations was found to be another major variable that can be controlled by T-line engineering and construction. The first of these configurations is indicative of two lines that might come into contact due to aeolian based line and pole movement (described in this test as “Parallel”). The second configuration was the “worst-case” fault in which the “Pigtail” end of a conductor was directly pointed to the other phase concentrating the arc in one location. Other independent driving variables of lesser control include the conductor sizes and materials (as mentioned above), fault currents, and the height above ground.

This particular part of this study attempts to quantify two main dependent variables

- Total particle counts by time; and
- Particles counts exceeding ignition temperature by time.

The FLIR is capable of tracking the temperature of the particles in specified temperature ranges; once the particles fall outside the lower part of that range, the FLIR is no longer able to detect the particle. The FLIR is able to detect particles above the temperature range, but temperatures are recorded as saturated at the maximum temperature of the calibration range. This made it difficult to examine in depth how particle temperatures changed over time as they fell (although not

impossible, and there is substantial information that can be gleaned from the thermal images). However, after evaluating multiple different components including particle velocity, raw particle temperature, and particle tracking, and trying to integrate data from two different types of tests ("Cage" and "Lift"), particle count and particle temperatures that exceeded paper ignition temperatures (approximately 451 °F) appeared to be among the most valuable dependent variables due to their usefulness in determining particle fire risk. These parameters also can act as a basis for other fire hazard aspects, specifically particle size, and a more accurate representation of particle temperature at ground impact. This is important because even a very small particle that exceeds the autoignition temperature of the surrounding fuel base can result in a fire.

The Lift tests were most representative of what might occur in the field, and therefore were of greater import for this analysis. Specifically, in the "Lift" components of the testing, when particle temperatures were not greater than paper ignition temperature, there were no fires observed, either with paper or the Cal-Fire test bed. Of critical importance here was that in almost all instances, low particle production and lower particle temperatures were associated with the smallest fault interrupt times (0.1 seconds, 0.25 seconds) and a correspondingly reduced chance of resultant fires (as seen in the Lift tests). Higher particle counts and higher counts of high temperature particles were strongly associated with longer fault interrupt times (0.5 seconds, 1.0 seconds) and resultant fires (again, as seen in the Lift tests).

Of further note, the number of total particles rose at a non-linear rate. We hypothesize that the distribution of particle size increases as more energy enters the system, and that a wider distribution of particles, including more numerous, smaller, hotter particles, are produced the longer the fault is held open. This phenomenon was not as apparent with 3/0 Cu, and may be due to combustion processes occurring with the aluminum and ACSR conductors.

This is borne out by two pieces of evidence. One is the large number of particles counted as the fault time increases. That they are small is evidenced by physics (small particles cool rapidly) and that they vanish rapidly from the FLIR's view field. The second evidence is an increase in the counts of particles that exceeded autoignition temperature of paper (greater than 210 °C) that survive the fall. These are either larger particles, molten particles, or burning particles (in the case of aluminum).

Total particle counts increase at a rate that appears to be based on a square function of fault interrupt time, especially for higher energy tests; this points to the importance of attempting to reduce fault interrupt times as much as possible in order to reduce fire risk. The implication for this is that reducing fault interrupt time, either through modifications of existing protective relay settings or the addition of protection class communications such as fiber optics into the protection scheme, has the potential to significantly reduce the chances of particle based autoignition of fuel sources surrounding conductor corridors in a non-linear fashion.

A discussion of particles sizes and their overall relationship to the volume of the material are discussed below in the body of the report.

Suggested next steps are to attempt to place the work found here into physics-based models and to extend the models developed here to a more generalized model that can be used for any conductor type or size. In addition, the impact of combustion on particle production and destruction cannot be ignored. For small particles, the ignition temperature for aluminum is greatly reduced, and can produce small burning particles, albeit with limited lifespans.

2 TESTING METHODOLOGY

Testing took place over a two-week period form October 2, 2019 through October 15, 2019 to cover a series of fault conditions. For this portion of the test, in order to capture the particles and explosions for thermal imaging, a FLIR thermal imaging camera was rented for the two-week duration (model A8303sc). The FLIR thermal imaging camera has the ability to capture 60 frames per second (fps) over a view frame of 714 by 1280 pixels. In order to capture the largest view field possible, the FLIR was placed on its side. Since the FLIR camera was a new addition to the test, it was unknown what would be found as the result of its usage at the end of the tests. The FLIR camera was experimented with over several trials until the system could be properly initiated.

Two test phases were examined. The first test phase occurred in the high current yard Cage, and occurred at average amperage test currents of 1000, 4000, and 7000 amps. Testing evaluated conductor configurations of phase to phase currents using a Parallel and Pigtail type conductor configuration. Several heights for the “Lift” phase of the test were tested in the high current yard until the final test setup configuration of 40 feet was used for the remaining portions of the test.

Initial test configurations included the following conductor type and other setups:

- Conductors: #4 ACSR, 397 MCM Al, and 3/0 Cu;
- Some specific tests simulating faults against steel infrastructure by different conductor types were also tested;
- Current Amperages:
    - 1000, 4000, and 7000 amps for the Cage Test;
    - 4000 amps only for the Lift Test;
- Conductor configuration: Parallel and Pigtail conditions
- Cage and Lift Tests
    - Cage Tests were approximately 10 feet above ground (indicative of flash zone)
    - Lift Tests were approximately 20 feet (initially) and finalized at 40 feet above ground (indicative of final fall zone from conductors in the field)
- Interrupt times were controlled to be approximately 0.1, 0.25, 0.5, 1.0, and 1.5 seconds
- Distance between conductors
    - Not used in final analysis due to the introduction of too many variable types.

Fuse wire was used in some tests to initiate the fault, but not all tests. The use of fuse wire is deemed to have minimal or no impact and was therefore not used in final analysis.

Figure 1 shows the overall “Cage” test arrangement. The conductors under test are placed at height at approximately 10 feet above the floor. The “Cage” test gives a view of the initial fault conditions, and tests were run at 1000, 4000, and 7000 amps. 40 lb[1] Kraft paper was spread beneath the conductors in order to observe if fires occurred; however, any fires here are unrealistic of potential fires in practice, as the sparks produced undergo significant cooling due to advection and radiation heat transfer as they fall (as well as potential combustion in some cases).

Figure 2 shows a conductor in the “Cage” setup, in Parallel mode. In some instances (especially during Parallel tests) a copper fuse wire was used to help initiate the fault. This was due to Parallel

[1] The weight of paper is based on how much 500 sheets (or a ream) of paper weighs in its basic unit uncut size. Kraft paper is based on 24” x 36” dimension, and can be designated as lb or #.

modes where the conductors were placed too close to each other welding into place, so the conductors were separated so as to avoid the welding issue. Typically distances that separated conductors for Parallel modes were 2-3 inches. The copper fuse wire did not seem to have any appreciable impact on test results. The 21kV electrical sources coming from the bushings on the cage wall were wired to opposite corners of these parallel conductors to prevent the arc from traveling off to either end of the setup (the magnetic force of the source currents push the arc away from the source).

Figure 1. Overall view of “Cage” test setup.

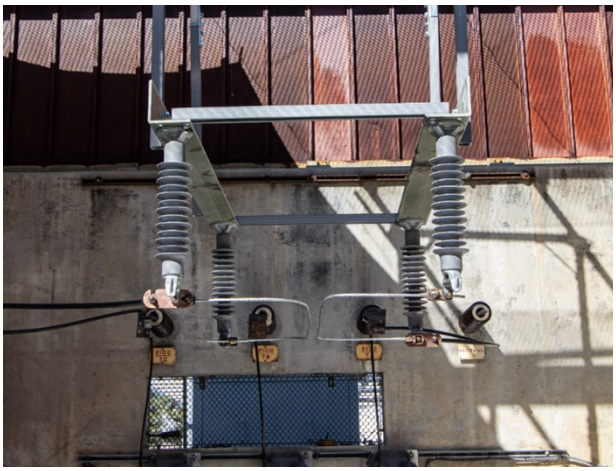

Figure 2. Parallel conductor configuration in “Cage” test.

Figure 3. Pigtail conductor configuration in “Cage” test.

Figure 4. Pigtail conductor configuration in “Cage” test, testing against a leg simulating a steel transmission line component.

Figure 3 shows an example, again in the “Cage”, of a Pigtail configuration. The Pigtail configuration is designed to simulate a dead-end line that might impact against a nearby line. It is considered a worst case scenario for fault conditions. In Pigtail configurations, the dead-end edge is placed perpendicularly 0.125” to 0.375” from the opposite conductor. **Figure 4** shows the Pigtail conductor configuration during the “Cage” test, with the Pigtail placed perpendicular against a steel leg simulating a steel transmission line tower component. These tests were designed to show the impact of a fault that might occur against a transmission line tower.

Figure 5 shows the overall view of the “Lift” test configuration. The “Lift” test was designed to look at various heights of different faults, with the fault current only occurring at 4000 amps. For the “Lift” tests, initial tests began at 18 feet, with the lift being raised up higher for subsequent tests. Eventually it was decided to leave the lift test configuration at forty feet, which is the maximum height we could achieve that is a compromise between distribution and transmission conductor heights. The test bed for many of the tests was a standardized Cal-Fire approved fuel bed (dried grass). For the remaining tests, 40 lb white virgin kraft paper was used as the test bed. These are also shown in **Figure 6**. Although not Cal-Fire approved, it made it easier to see even small singe marks and fires, as well as to look at the remains of particulates of the fault explosion. For the vast majority of tests, the FLIR camera was situated at the lower, right hand side of **Figure 5** (Red Square).

Figure 5. Lift test environment, showing location of FLIR Camera.

(a) **(b)**

Figure 6. Lift test environment, showing kraft paper test bed (a) and Cal-Fire approved test bed (b).

Figure 7 and **Figure 8** show examples of FLIR image output for the Cage and Lift, respectively. FLIR images in the Cage were able to capture the plasma cloud and explosion center for the majority of cases. Lift images were not able to capture the plasma cloud or explosion, since it was out of the view field of the thermal imaging camera. The view field only captured the lowest portion of the falling particles (the particles closest to the ground surface), as this part of the test was focused on the evolution of the particles as they fell. FLIR ATS files (ATS files are the native data storage protocol for FLIR, and not to be confused with ATS the facility) took up approximately between 0.7 and 1.2 GB of data space per test.

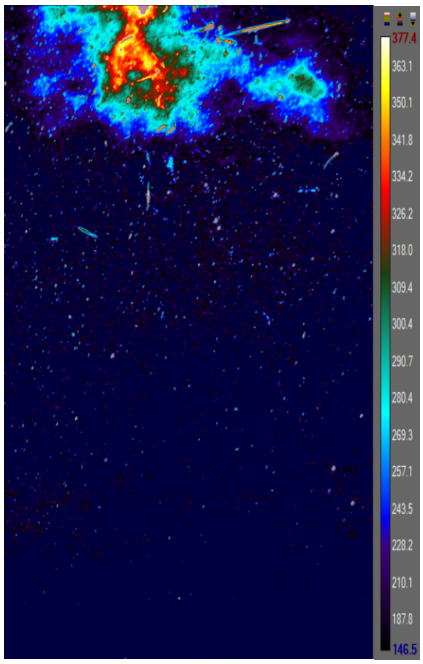

Figure 7. FLIR Image, Cage Test.

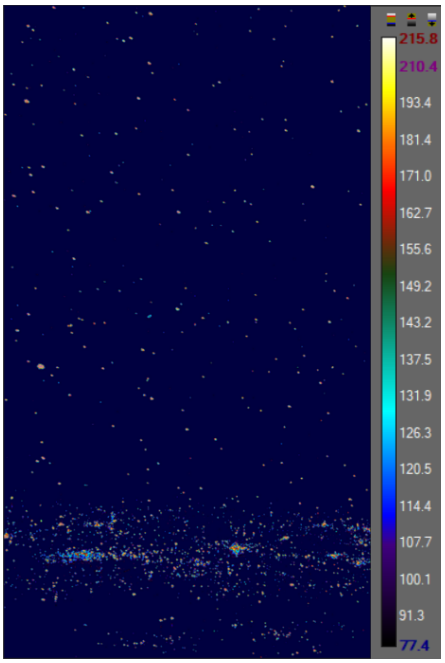

Figure 8. FLIR Image, Lift Test.

3 DATA ANALYSIS

Data was assessed in multiple ways. Each image was visually assessed post-test to look for details for data exploration. By doing so, both for the Cage tests and the Lift tests, the initial image frame for the test fault could be determined. For the Cage test, this was easy; the fault was easily observable by frame. For the Lift results this proved more difficult. After careful observing of both the temperature imaging and counts image, it was found that the initial explosion flash was always visible as reflected heat on background components in the counts image. The frame was then noted in the database as the initial time frame of the fault. During this run through of the videos, the imaging was assessed for observable fires. Fires occurred on both the Cal-Fire approved test bed and the Kraft Paper (the thermal imaging did not make it clear as to which test bed was on the ground for the test); If fires were observed, this was noted. Later, the videos with fires were re-examined to count the number of fires that occurred. In the database, each test was given an identifier that described the day, month, and year tied to the hour and minute of the fault (and given a test number as well). Thus, a test taken on October 4, 2019 at 12:32 PM is identified as 10042019_1232051, where the 051 is indicative of the test number as given in the lab.

The thermal image videos were also revisited several times after programming of image analyses was started as several different spatial and temporal flag points were needed for input to the program. These included for the Cage data when the flash finished, the lowest extent of the flash, and when it became evident that a particle floor had to be developed, finding the point where the particles would hit and accumulate, and creating a “base” that wiped out these from the image analysis, as well as particles that would bounce and add to the accumulated particles (artificially increasing the number of particles in a count).

Each image was imported as a set of pixels, and then excess pixels were stripped away through the algorithm so that only one pixel was tracked per particle. Where excess pixels were removed, the total count of these pixels were tracked in the database for possible future assessment of particle “sizes”. Initially, attempts were made to make use of algorithms available on the Mathworks website, but these algorithms ended up being overwhelmed even by the relatively few particles associated with the Lift tests. This course was abandoned and a special algorithm was developed that took advantage of newer toolsets available in the Mathworks toolkits. The algorithm would create a “cut set” of particles per image, and then would use the particle positions at time ***t*** as a starting point to search for the particle’s movement at time ***t + 1***. Each particle was given an identifying ID, as well as having characteristic properties determined for the pixel (time ***t***, elevation, rounded elevation, temperature, temperature distribution, particle size, particle location, particle location at time ***t + 1***, relative particle velocity (pixels/second) as well as an approximate real velocity, in addition to an identifier of the test.

Particle counts by time gives an indication of how many particles are produced, how these particles evolve over time, and how many hot particles reach ground level based on conductor height. Particle count was determined to be based approximately on several basic input variables:

- Conductor type
- Fault amperage levels
- Fault interrupt time (duration)
- Distance that particles travel
- Particle fall time
- Conductor configuration (Parallel or Pigtail type fault)

The initial goal was to find a complete physics-based approach to examining particle “life”; however, for this phase the focus became creating an empirical model, based on experimental parameters and on conductor configuration and conductor type, that could show the number of hot particles that would reach the ground surface as a function of particle fall time, fault interrupt time, and fault amperage. Other input variables that were recorded during the testing such as use of a fuse and distance between phases were eliminated for the analysis due added complexity; their inclusion would have introduced too many variables to assess, and appear to be somewhat minor in their impact. To properly assess them, there would need to be substantially more tests runs performed.

Particle counts were examined for each type of test; however the tests were performed under two different FLIR calibration ranges. For the Cage tests and the Lift tests, the FLIR was set to a different temperature range (newer and more advanced FLIR cameras, not available for rental, have the capability of looking at multiple FLIR calibration ranges and alternating calibration ranges on a per image frame basis). A temperature range was chosen for the two major test conditions that would span both tests and have a chance at capturing characteristic particle temperatures. For the Cage test, a higher calibrated temperature range was chosen so as to capture a distribution of hot particles. For the Lift test, a lower range was chosen, as it was assumed that most particles would have cooled substantially over 40 feet (12.2 m) of fall distance.

Particle temperatures are recorded by identifying a specific particle centroid from the FLIR data output, and then determining a surrounding search area that incorporates the temperature recorded by the FLIR in each of the pixels of the centroid. The particle temperature is limited by the FLIR’s calibrated temperature range. Relative particle sizes are determined by a count of the pixels from the FLIR image that represent the particle. Finally, relative particle velocity is determined by a similar search routine that tracks the particle location, then searches below looking for a “nearest” neighbor for the next time step. Since the time interval for the FLIR system was 1/60th of a second, particles have various relative velocities based on distance to the camera (where nearer particles appear to move faster and particles to the rear seem to move more slowly).

The resultant output of this was approximately 7.5 million points particle points tracked and analyzed over 75,000 FLIR camera IR images. Temperature ranges assessed differed across the two tests, which restricted direct one-to-one comparison (the newest FLIRs that don’t have the calibration range limitation were not available for rent). The Cage FLIR temperatures ranged from approximately 145 °C to 380 °C. This resulted in any particle that dropped below 145 °C “vanishing” from the FLIR view field. For the Lift FLIR temperatures observations, the range was from 80 °C to 215 °C – any particle below 80 °C vanished from the view field of the FLIR thermal imaging. For both of these image sets, any temperatures above the maximum temperature of the range would be “saturated”, i.e. it would still be visible, but the actual temperature would be recorded as greater than 380 °C for the Cage images and greater than 215 °C for the Lift image observations.

Data was initially analyzed for apparent particle velocity and temperature trend, with the intent to develop experimental ranges of heat transfer coefficient. However, after consideration of the output, this was still a goal of the effort, but it is believed not to be immediately useful to the System Protection group as a usable tool.

After examining the data in multiple permutations, two different approaches became relevant for determining future risk assessments for System Protection. The first approach looks at the

particles as having a lifespan, with the lifespan defined as being visible by the thermal camera. Although this is not exactly accurate, it leads to a single equation for each conductor material and fault configuration that gives particle count as a function of time, interrupt time, and input current.

The second approach looks at all the particle temperatures and counts the number of particles exceeding the autoignition temperature of paper. This temperature (210 °C) was determined after a review of literature and was found to be slightly below the autoignition temperature of paper (range of 218 °C through 246 °C, Graf, 1949) and is coincidentally at the high end of the temperature range for the Lift tests. It is consistent with the ignition temperature of dry grass as well. Of course, is a complicated phenomenon, as the autoignition of dry grass is dependent upon multiple factors that can include wind speed, relative humidity, and moisture content of the grass.

For the sake of conservatism, it was set at 210 °C, counting particles that might be in the range 210 °C through 215 °C and greater. Therefore, a continuous range of particle counts can be determined as an autoignition risk. This assessment was also examined to see if any of the lift tests that didn't have particle temps above 210 °C would result in fire. The temperature used here is definitely on the low end of that range. However, due to the calibration range for both sets of tests (Cage and Lift), the 210 °C is at the highest bound that is shared by the FLIR camera for all tests.

Table 1: Fires/No Fires Resulting from Lift tests, 4000 amps, Kraft paper or Cal-Fire Test Bed.

Conductor	Configuration	0.1 s	0.25 s	0.5 s	1.0 s
397 MCM Al	Parallel	No Fire	N/A	No Fire	No Fire
	Pigtail	No Fire	N/A	Fire	Fire
#4 ACSR	Parallel	No Fire	No Fire	Fire	N/A
	Pigtail	No Fire	No Fire	Fire	Fire
3/0 Cu	Parallel	No Fire	N/A	No Fire	Fire
	Pigtail	Fire	Fire	Fire	Fire
Angle Iron-397 MCM AL	Parallel	No Fire	N/A	No Fire	Fire
	Pigtail	N/A	N/A	N/A	N/A

Table 2: Fires/No Fires Resulting from Cage tests, 4000 amps, Kraft paper or Cal-Fire Test Bed.

Conductor	Configuration	0.1 s	0.25 s	0.5 s	1.0 s
397 MCM Al	Parallel	No Fire	No Fire	No Fire	No Fire
	Pigtail	No Fire	Fire	Fire	Fire
#4 ACSR	Parallel	No Fire	N/A	Fire	Fire
	Pigtail	No Fire	Fire	Fire	N/A
3/0 Cu	Parallel	No Fire	N/A	No Fire	No Fire
	Pigtail	No Fire	No Fire	No Fire	Fire
Angle Iron-397 MCM AL	Parallel	No Fire	N/A	No Fire	Fire
	Pigtail	No Fire	N/A	Fire	Fire
Angle Iron - Steel Armor Rod	Pigtail	No Fire	N/A	No Fire	Fire

Since the Lift tests are most representative of actual fall heights, this assessment only examined the 4000 Amp combined Cage and Lift results, and looked only at whether the Lift particles created a fire. Fire is determined by whether flame is observed in the thermal camera video history, for both the paper and Cal-Fire fuel bed.

Table 1 and **Table 2** summarize the result of each test category and whether a fire occurred, both for Cage and Lift testing. The only fire that resulted at 0.1 second for the Lift occurred with copper for the Pigtail testing. Fire resulted for all fault times for copper Pigtail testing. In contrast, for the copper Parallel tests, no fire was detected for 0.1 or 0.5 second fault time. Fire occurred at 1.0 second of fault time. No data was available at 0.25 second.

For 397 MCM Al, no fire was detected for 0.1. 0.5, or 1.0 second fault time for Parallel testing. For the Pigtail testing, no fire was observed at 0.1 second, but fire was observed at 0.5 and 1.0 seconds. No results were available for 0.25 seconds fault time.

For the #4 ACSR, no fire was observed for either Parallel or Pigtail for 0.1 and 0.25 seconds fault time. For both Parallel and Pigtail, fire was observed at 0.5 and 1.0 seconds fault time, with no results available for Parallel at 1.0 second fault time.

There were no Pigtail results for Angle Iron-397 MCM Al, but for 0.1 second and 0.5 second fault time, no fire was observed for Parallel testing. Fire was observed at 1.0 second, with no test results available at 0.25 seconds fault time.

For the Cage testing, for both Pigtail and Parallel, no fire was observed for 0.1 seconds. However, fire was observed for the lift Cu Pigtail experimental runs (which had fire for all tests). Again, 397 MCM Al Parallel is fire free for all fault times, as is 3/0 Cu (there being no data for 0.25 seconds fault time). There is likely not enough data to support a rigorous statistical analysis.

Overall, given the data on hand, the chance of fire occurring increases as the fault time increases, and are higher overall with Pigtail configurations than with Parallel configurations. Only 397 MCM Al, Parallel configuration, had no observations of fire for both the Cage and the Lift tests. Based on the above tables, for Cage results Pigtail configuration had a 50% chance of resulting in fire. For the Parallel configuration, the Cage had an approximate 25% chance of resulting in fire. For the Lift testing, approximately 73% of the Pigtail configuration summaries resulted in fire. Matching the Cage, for the Parallel configuration, there was a 25% chance of fire. All these chances of fire increase as the fault time increases.

4 PARTICLE COUNT ESTIMATES

After initial analysis of the data sets, it was ascertained that for the 4000-amp tests there seemed to be sufficient corresponding data between the Cage tests and the Lift tests to “combine” the results. **Figure 9** shows an example of this for the #4 ACSR Pigtail test (with 0.125 in through 0.1875 in of separation) for six different tests at 4000 amps. Particle counts for the Cage and Lift tests were combined by assuming that the Cage particles begin falling near a 40-foot (~12m) height, with Lift counts assumed to be based on ground level, and so used the height of the lift to determine the total fall time. **Figure 9** shows results for 0.1 sec, 0.25 sec, and 0.5 sec fault times for Cage and Lift Results. In **Figure 9**, particle counts fall off exponentially over distance as the particles fall closer to the ground surface, but not in a way that is immediately straightforward to model. The six different tests appear to form imperfect pattern trends (0.1 sec, 0.25 sec, and 0.5

sec seem to be “continuous”, This pattern, with some exceptions, repeats itself in the other 4000-amp tests for Cage/Lift equivalent test pairs for the rest of the conductor types and configurations.

Figure 10 shows the same data transformed into a calculated time domain. The data encapsulated in **Figure 9** and **Figure 10** by the blue tinged box are Cage Test results, while the data encapsulated by the yellow tinged box is the Lift results. Several assumptions are used here, among them that the particles are assumed to start falling with a zero initial velocity (there is no initial velocity imposed on the particles by the fault explosion), and that smaller particles are not slowed appreciably by air drag forces, or born upwards by thermal natural convection effects. In addition, it is assumed that all particles are created simultaneously at time t=0. The time equivalent of 1.58 seconds on all subsequent figures is the equivalent time for ground level of 40 feet. In the tests, the particles don’t necessarily reach ground level; in the data analysis a portion of the lower section was excised due to view field considerations and particle bouncing that created problems with analysis.

The particle fall-off as seen in **Figure 10** can be approximately modeled as individual exponential functions to the form of:

$$P(t) = A\ exp(-\tau t)$$

Where:

***P*(*t*)** is particle count as a function of time;
A gives the maximum particles produced (as a function of the individual regression for each line);
τ gives the resultant time constant for particle “life”; and
t is fall time.

Figure 11 gives an example of the combined Cage and Lift data for #4 ACSR, Pigtail, at 0.1 second fault, for 4000 amps. An exponential regression formula of the form:

$$P(t) = 4883.2\ exp(-3.579t)$$

is developed, with A above becoming 4883.2 and the time constant for particle life, **τ**, being 3.579/s. The particle life time constant is based on the 4000 amp data; there was insufficient data for the 1000 and 7000 amp results. For all of the different exponential equations, **τ** was linearized into a single equation as a function of fault interrupt time that gave a single slope for each set of three fault interrupt times. The increase in particles as a function of interrupt time impacts particle count in a clearly non-linear manner; although there may be a clear reason for that (to be discussed later). It was eventually found that ***A*** could be approximated a function of the interrupt time, *f*, resulting in the final equation for particle “life” as a function of time as:

$$P(f,t) = A(f)\ exp(-\tau(f)t)$$

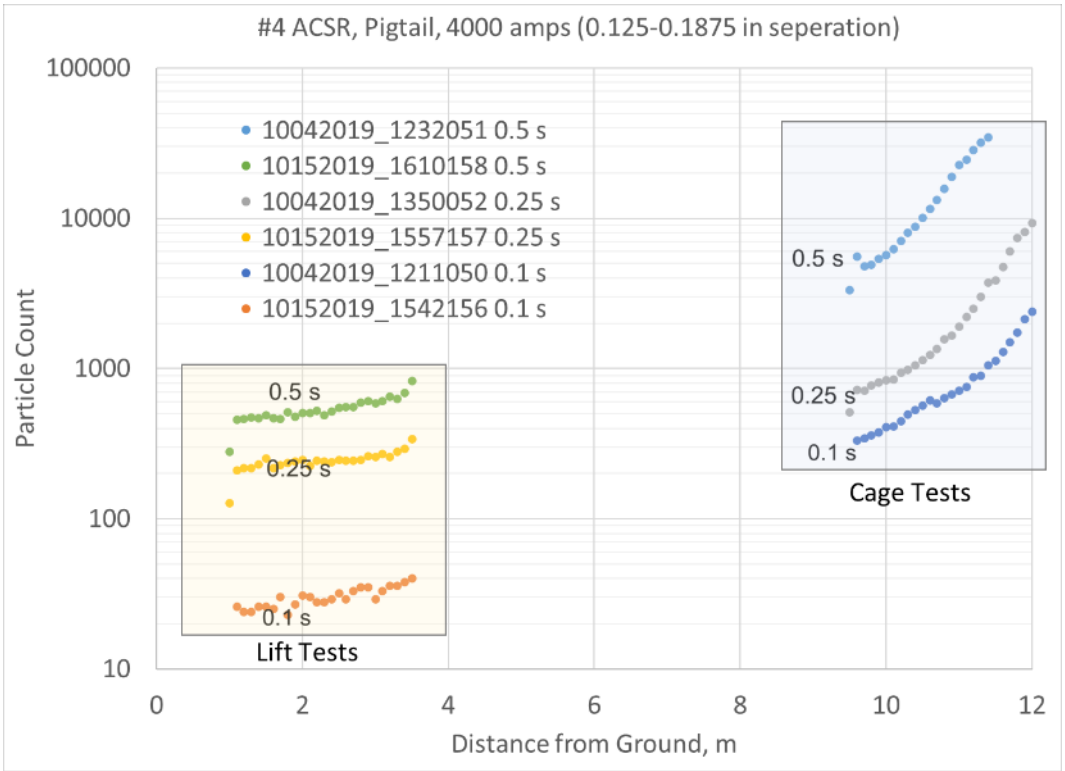

Figure 9. Particle Count vs. Distance from Ground (m) for six different fault tests, #4 ACSR, Pigtail Configuration, with three different fault times (0.1, 0.25, and 0.5 s).

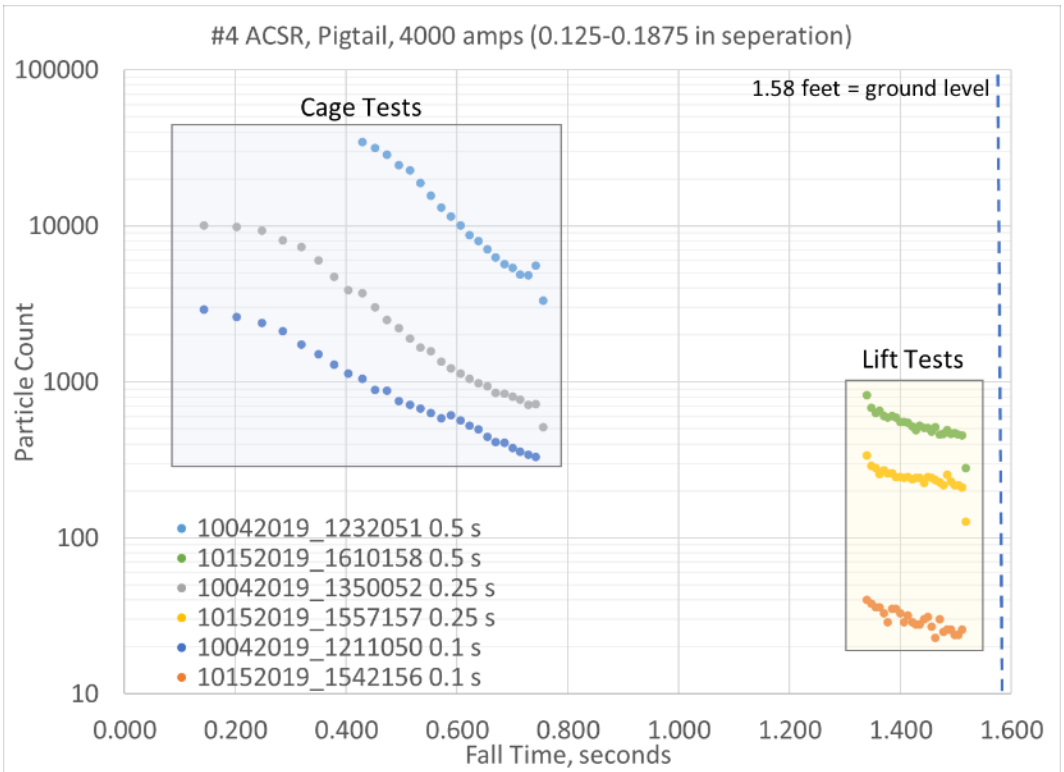

Figure 10. Particle Count vs. Fall Time (seconds) for six different fault tests combined into three different fault times (0.1, 0.25, and 0.5 s) for #4 ACSR, Pigtail Configuration.

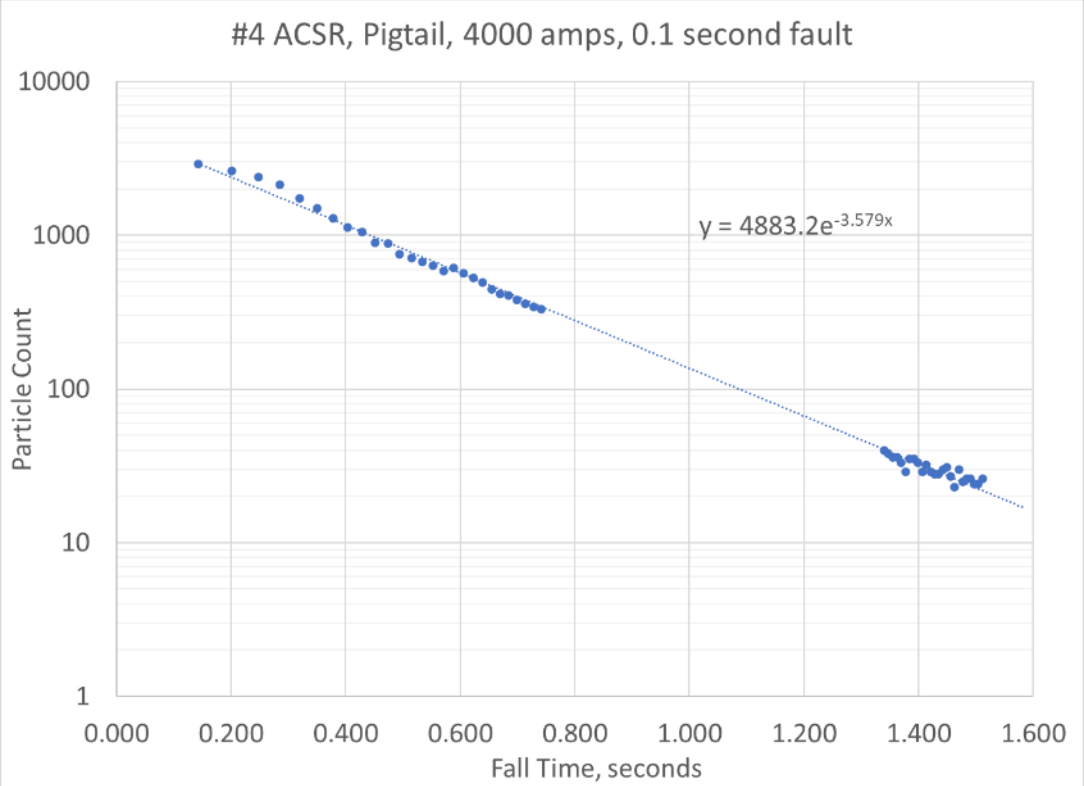

Figure 11. Particle Count vs. Fall Time (seconds) for the Cage and Lift tests combined, 0.1 second fault time, for #4 ACSR, Pigtail Configuration.

For the Parallel configuration, copper did not produce any fires for the Lift tests. In contrast, out of all the six tests at 0.1 seconds fault time for the various conductor materials and configurations, the copper Pigtail tests produced the only fire, and produced fires for the 0.25 s, 0.5 s, and 1.0 s fault times as well. Copper Pigtails showed melting of the Pigtail conductor (not of the looped conductor) showing the extreme heat that is produced in the Pigtail tests as opposed to the Parallel tests. With the focused energy acting to melt the copper at the end of the Pigtail, copper's higher melting point, and copper having a higher specific heat and releasing less energy during the fall than the aluminum particles (those that are not burning), overall particle temperatures were likely significantly higher.

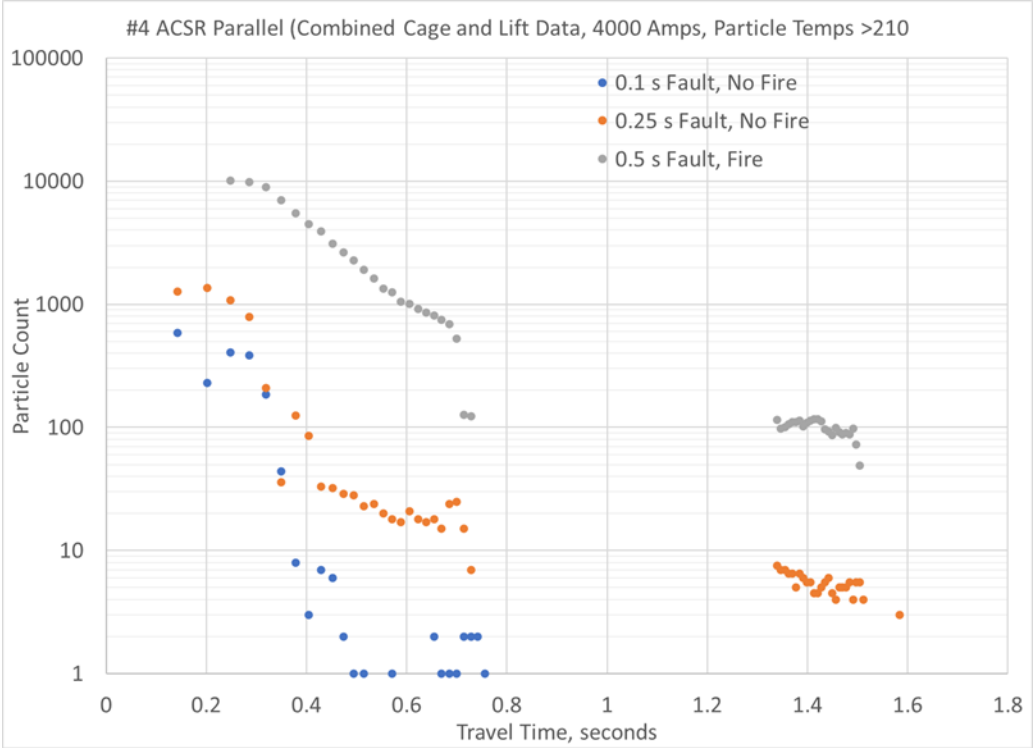

Figure 12. Particle Count vs. Fall Time (seconds) for #4 ACSR, Parallel Configuration, 4000 Amp combined tests, particle counts only for particles >210 C.

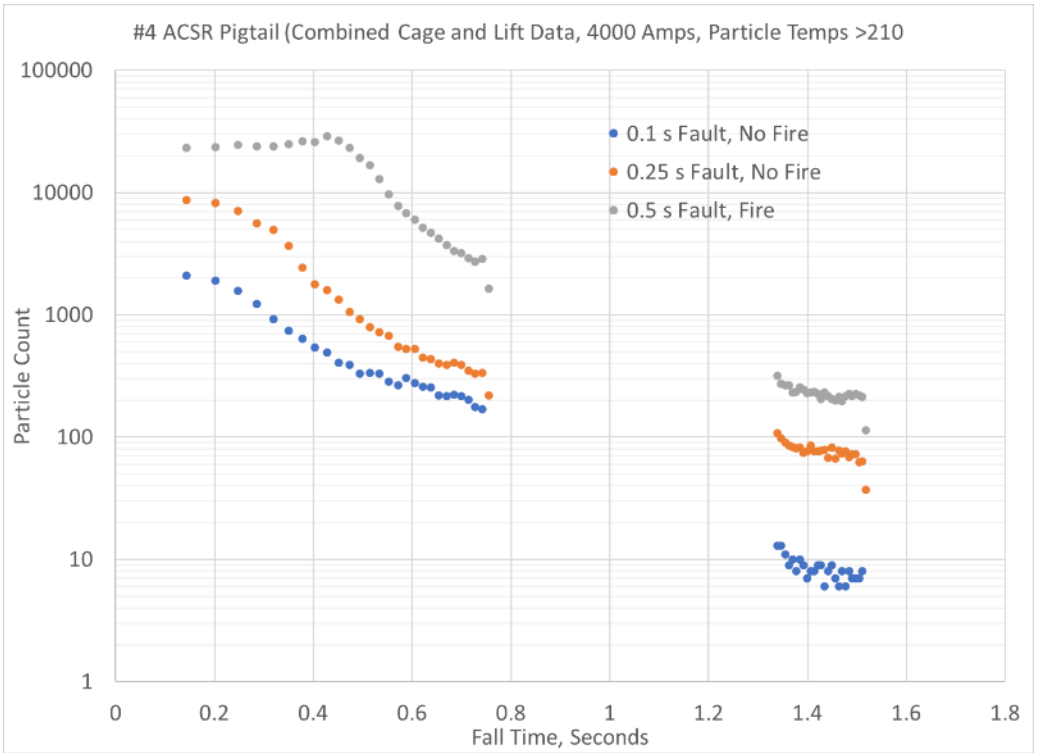

Figure 13. Particle Count vs. Fall Time (seconds) for #4 ACSR, Pigtail Configuration, 4000 Amp combined tests, particle counts only for particles >210 C.

5 DISCUSSION

For all faults, several events occur. Upon contact between conductor phases, there is an exceedingly bright flash, which creates an ultra-hot plasma cloud as the parts of the conductor are vaporized. Tests have shown (Wilson, 1955) and were confirmed qualitatively in these experiments, that substantial conductor mass is converted into hot gases. This is especially true of aluminum, which has a tendency to combust in the presence of oxygen. Copper and steel do not have this tendency to burn as does aluminum. For an aluminum conductor fault, **Figure 14** through **Figure 15** shows the evolution of a plasma cloud during the fault as seen in the first 20 frames of the FLIR thermal imaging, taken at 60 fps. Other faults (including ACSR and copper) show similar sequences; some with more spectacular plasma clouds, some less so. The brown areas seen in the center of the plasma cloud are temperatures that exceed the maximum temperature of the camera range calibration. The plasma cloud rapidly cools as it expands, until finally all that are left are individual hot particles as seen in **Figure 15**.

For aluminum, these particles are made up of three different types of materials, all of which can be described in general as sparks. One is hot aluminum debris that resulted from the initial fault. The second is molten aluminum, melted as a result of the fault explosion. Finally, there are actually burning alumina particles. These are very small; their lifecycle is described in detail in Mills, 1984. During their burn cycle, they stay at temperatures close to the combustion temperature of aluminum and oxygen, and have temperatures that greatly exceed that of the molten aluminum droplets.

Neither copper nor steel are expected to combust; aluminum has specific properties that can result in easy and complete combustion at much lower temperatures, and indeed is a primary component of some solid rocket fuels. Jacobson et al (1964) discussed in detail the flammability and explosive potential for metals. Aluminum was found to have Severe Ignition and Explosibility, where copper was found to be Weak, except for powders, and these tended to ignite in furnaces and not due to spark or flame source. At higher oxygen levels, copper's ignition temperature drops, but no good evidence was found for ignition at ordinary atmospheric pressure and makeup. Trunov et el (2005) found that very fine aluminum powders with a large specific surface ignite at much lower temperatures than bulk aluminum samples, and both aluminum nano-powders and flakes were observed to ignite at fairly low temperatures, between 560 C and 800 C. The work showed that particles of similar sizes were observed to ignite at very different temperatures. **Figure 18** shows experimental data for different particle sizes and ignition temperatures.

For the copper tests, there should only be vaporized copper and hot copper particles, with no burning components. Some small melted copper balls were visible from remaining particulates found on the ground; however, the copper conductor itself did show excessive signs of melting. During the Pigtail tests where the energy was highly focused the tip of the Pigtail was melted, appearing like a candle. Aluminum (both MCM and ACSR) will have burning particles, molten particles, and very hot non-molten particles, with evidence of all three collected (including what looked like ash particles, which were not visible after copper tests). Aluminum Pigtail conductors, in contrast to the Copper, were burnt away, as much as an inch in MCM aluminum, as opposed to the melted candle look of the copper.

In tests in the ATS High Current yard, the faulting flash and resultant sparks smoke cloud were larger the longer the interrupt time. Glowing sparks fall towards the ground; substantial alumina, steel, and copper particles were found after each test. But only in the case of aluminum would there be molten blobs to be found on the ground surface.

From a physics point of view, the faulting arc creates enough energy release to raise the conductor surface to a boiling point and to then vaporize a significant part of that. The aluminum vapor forms a burning plasma cloud upon contact with the oxygen in the air.

Mills (1984) reports that the pressure underneath the fault arc "can be as high as two or three atmospheres, and hence the metal surface can attain a temperature in excess of the normal boiling point, which is 2,730 K." This high pressure then acts to eject molten aluminum as small droplets. The normal ignition temperature for an aluminum droplet is approximately 2,300 K, which is also approximately the melting point of aluminum oxide. For any temperature below this a solid oxide layer inhibits the chemical reaction of oxygen and aluminum, resulting in a relatively slow oxidation process, with the particle cooling purely as a combination of convection and radiation heat transfer in a process that can be modeled as a lumped capacitance model. However, for very small particles, Trunov et al., (2005) found that aluminum particles can ignite and burn at sizes of less than 10 mm to 100 mm (**Figure 18**). There is then a step change where the particles burn at the expected ignition temperature for aluminum. It is these smallest particles that can represent increased fire hazard. How many of such particles are produced during an arc is unknown, but during the testing substantial smoke was observed, as well as substantial mass loss of the aluminum cable (especially during pigtail tests). It is likely that much of the smoke was produced from burning aluminum; certainly there was very little aluminum detritus visible, even under the more controlled Cage tests, that would represent the amount of mass lost in Pigtail aluminum tests.

Figure 19 shows two typical Pigtails from testing. The Cu 3/0 Pigtail (right) has a half melted look at the end. The MCM 397 Al Pigtail (left) shows significant loss and a pitted, not smooth surface, as though there was substantial boiling and burning of the aluminum. Both pigtails were marked at the same point from the end. This rather remarkable result seems in keeping with Mills (1984) and other work, and shows that aluminum particle production (and possible particle fire) is a much more energetic process than that found in copper. The additional energy could of course only come from combustion.

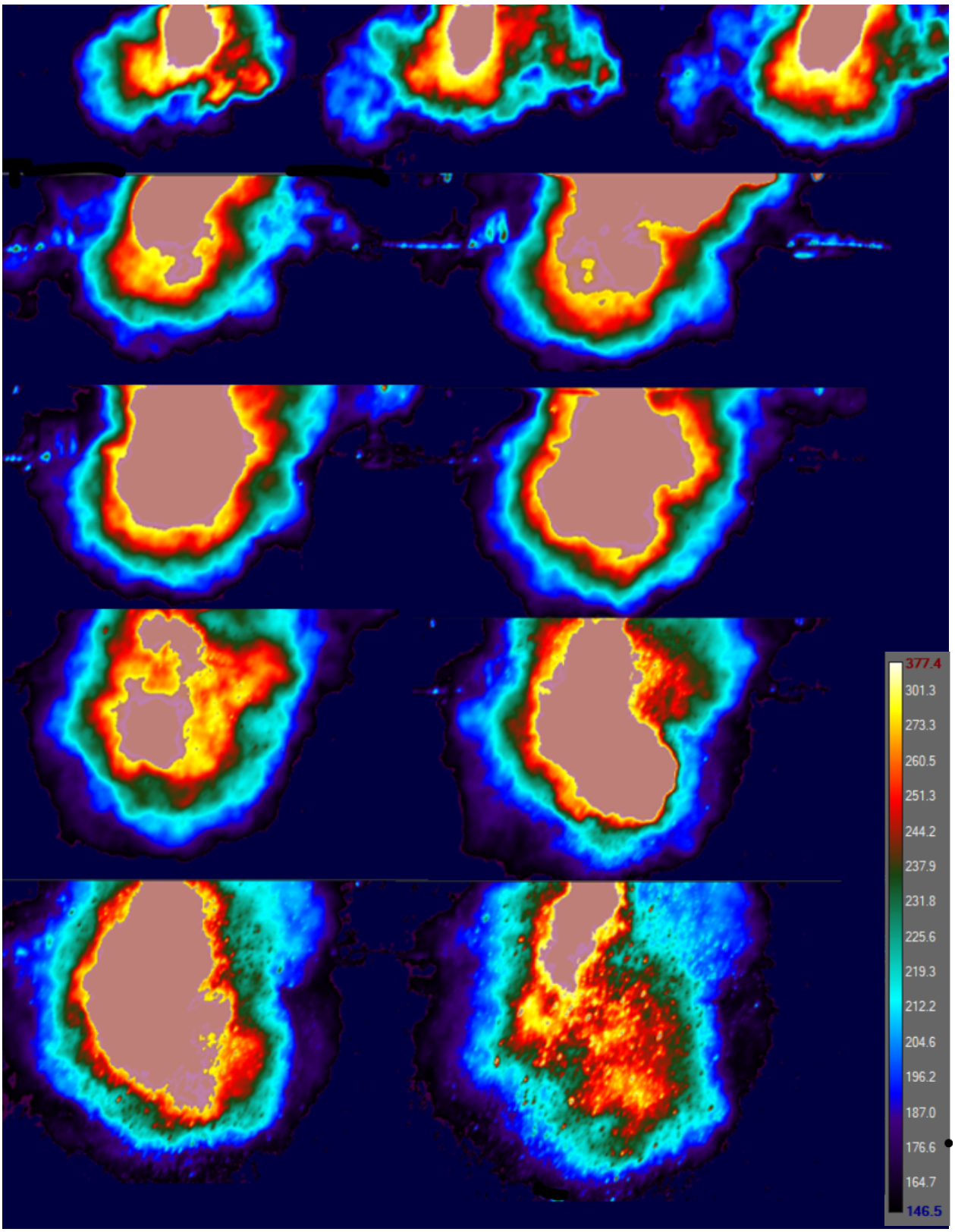

Figure 14. First eleven Frames of fault (frame rate 60 fps).

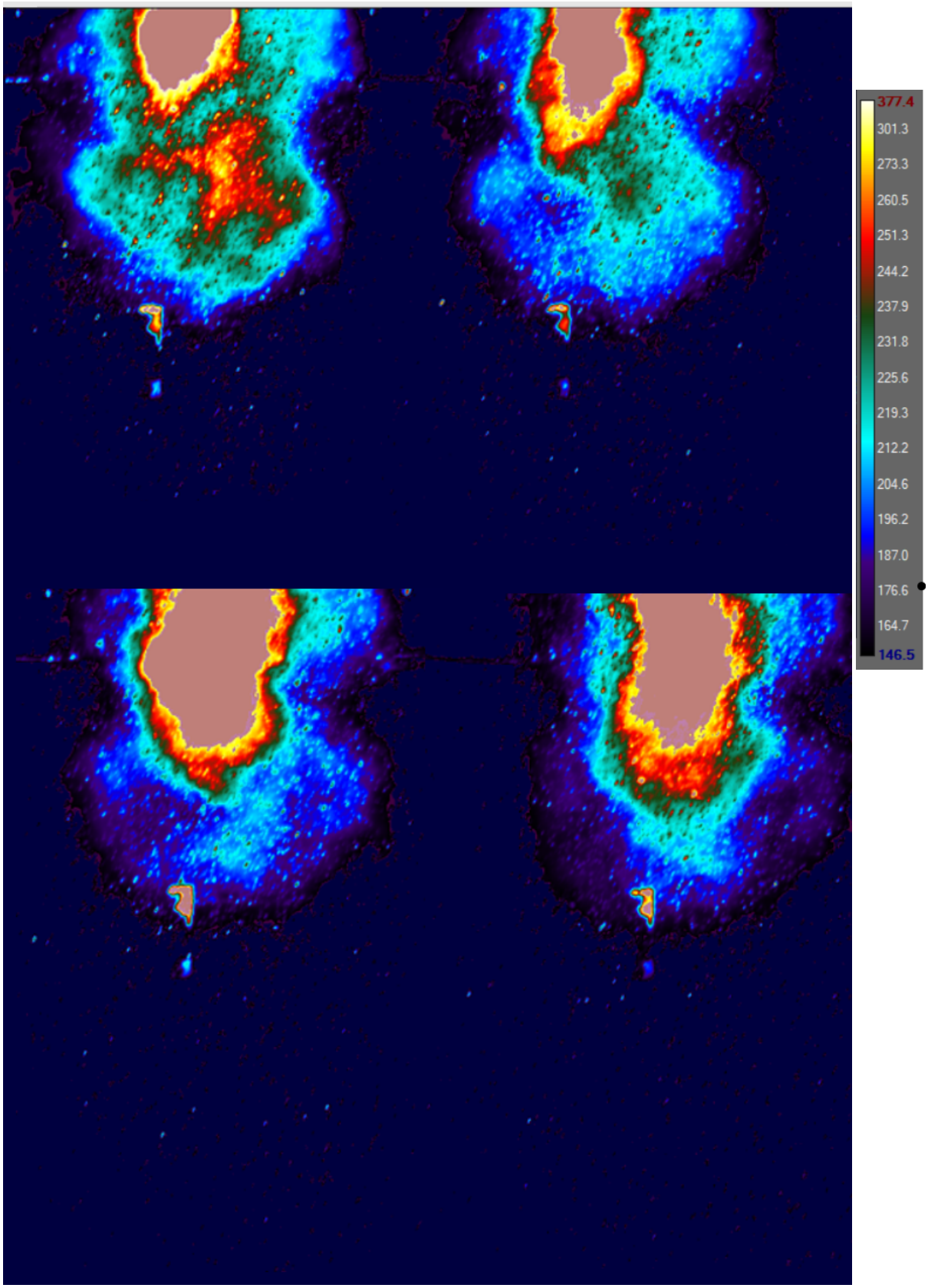

Figure 15. Frame 12 through Frame 15 of fault (frame rate 60 fps).

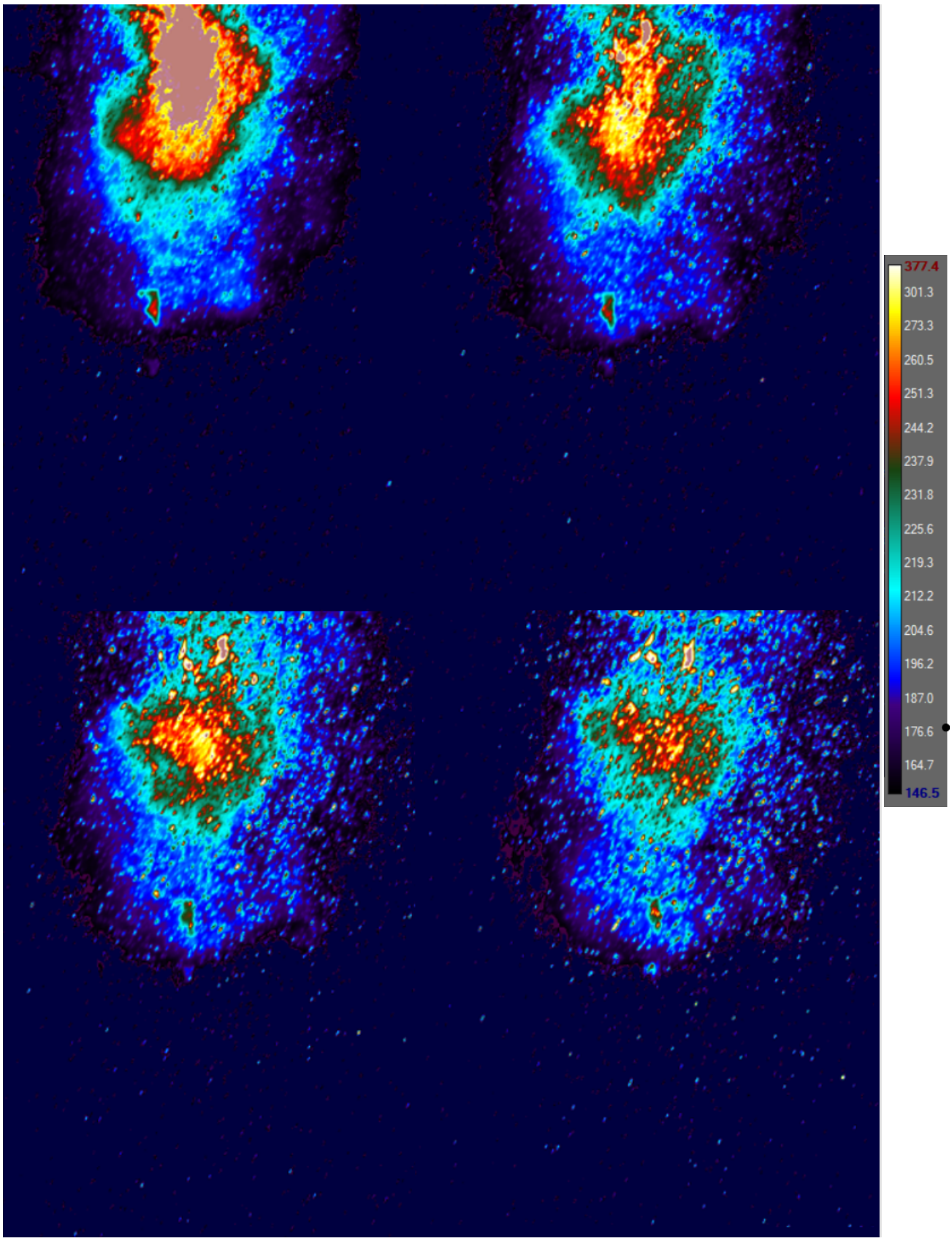

Figure 16. Frame 16 through Frame 19 of fault (frame rate 60 fps).

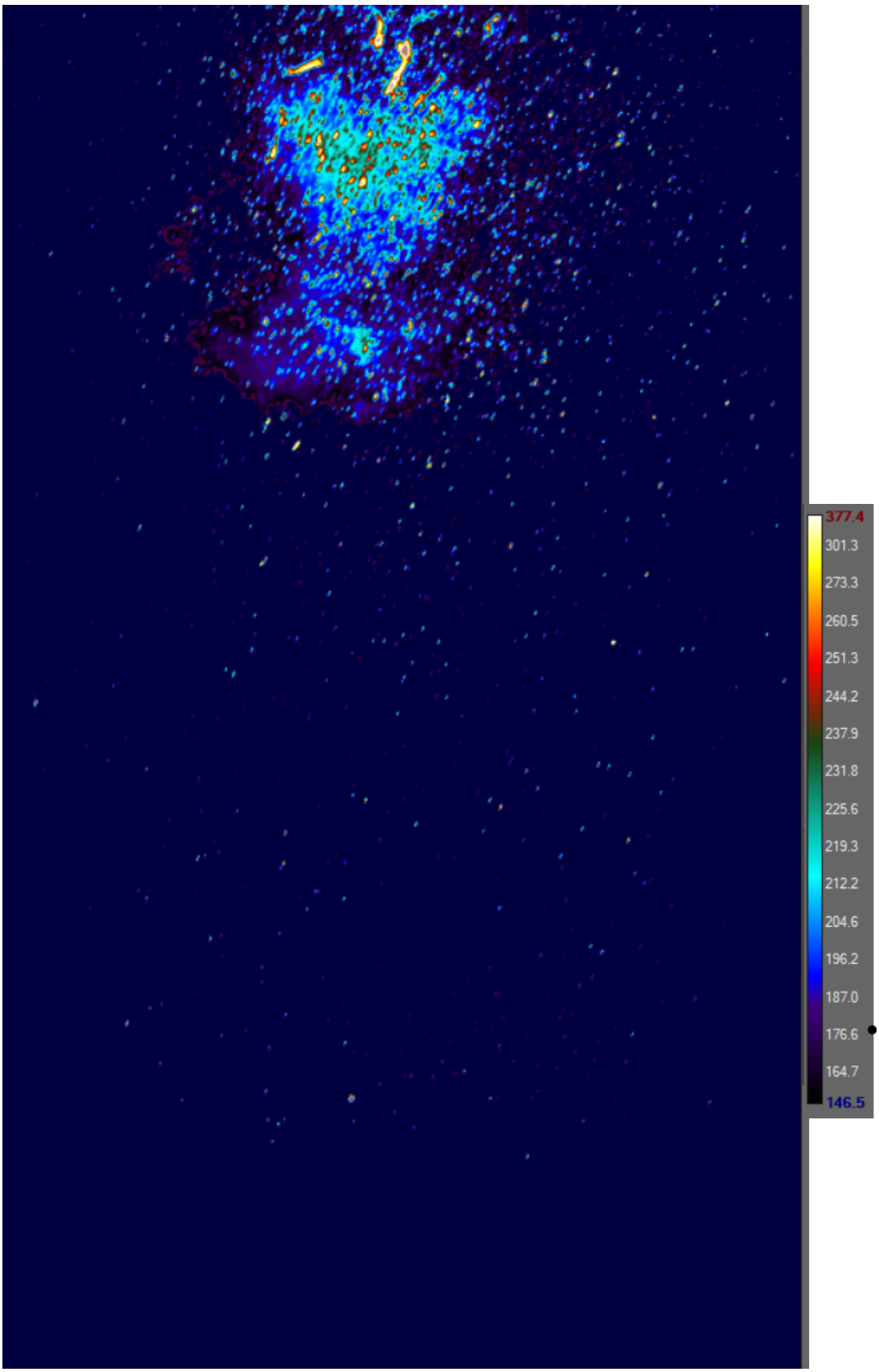

Figure 17. Frame 20 of fault (frame rate 60 fps).

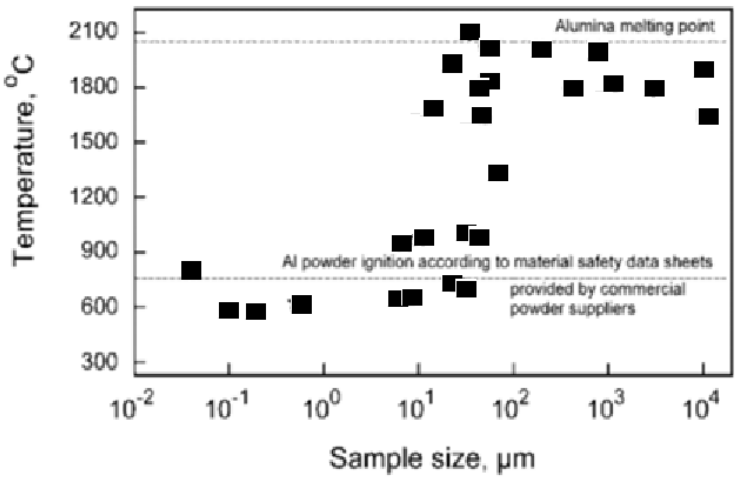

Figure 18. Experimentally determined temperatures of aluminum ignition as a function of the used sample size (Adapted from Trunov et al., 2005).

Figure 19. Comparison of typical aluminum (397 MCM Al) and copper (3/0 Cu) pigtails after fault testing. Both conductors were at approximately the same starting point prior to the test initiation.

Any analysis of the temperatures recorded by the FLIR will be assumed to be of particles of this type (i.e., cooling by radiation and convection alone), as a burning temperature would result in a rapidly burning, high temperature particle that would exceed the calibrated temperature range and result in saturation of the thermal image. This is not to dismiss the risk of burning particles, or to deny the existence of them in the testing. However, due to the limitations of the FLIR cameral, the thermal imaging was not able to confirm that burning particles occurred. There is a

great deal of evidence of very hot particles, however, including molten aluminum, and steel that had been transformed into small metal balls (as detected on the paper after some of the tests), a clear sign of melting. For molten aluminum particles, aerodynamic drag forces can act to expose unoxidized aluminum. Aluminum vapor escaping through high mass transfer rates from the molten surface can then result in a high steady state combustion flame front that balances the heat losses by convection and radiation. Slower particles should theoretically fall at a slower velocity, but the viewshed of the thermal imager results in enough uncertainty that any evidence of this would be dwarfed by change in scale created by the FLIR thermal imaging lens.

The reaction of aluminum and oxygen is highly exothermic. Significant energy is produced beyond that created by the fault arc[2]. The flame temperature of burning aluminum are very high and have been measured to be about 3,800 K. The burning will continue until the droplet is quenched by ground impact or the entire droplet is burnt, with the initial size of a droplet determining its lifetime. Mills found that only the largest burning droplets are able to reach the ground before burning up, and are themselves a minority of the total particles (Mills, 1984).

Due to their high temperature, burning or molten droplets have the highest fire ignition risk of all particles produced. This however does not eliminate non-molten hot particles from being a potential hazard to brush or other flammable material. The vast majority of particles that fall are hot metal that is not burning, but can still result in fire; this was explicitly seen in the copper Pigtail tests. Copper requires about 50% more energy than aluminum to rise to steel's melting point (assuming a cubic centimeter of material). ACSR requires about 20% more energy. This does not include potential energy from burning aluminum adding additional energy into the mix.

There is still an outstanding question as to the total particle production and the characteristics of the particles. Based on a particle "lifespan" equation, it may be possible to back-calculate a particle size distribution based on the lumped capacitance model. This is a non-linear first order differential equation of the form that incorporates both radiation and convection, and requires a computer program in order to assess. This further assumes that none of the particles are "burning" as indicated in Mills (1984), although it must be expected that some will be burning. If so, Mills states that burning particles are likely a small minority compared to molten and hot metal detritus.

6 CONCLUSION

Determining the physical basis for the maximum particle production is one that is still under development, but some issues have become clarified. The longer the current flows (i.e., the longer the fault time), the smaller and the hotter particles that are produced, and therefore the longer the lifespan. This is especially true for aluminum, where aluminum particles igniting and burning can lead to an increase in overall energy pouring into the system, taking a process that might be based only on input energy alone (amperage squared) and adds into combustion energy as well. The particle production is stochastic and highly variable; however clear trends are visible.

As more energy pours into the overall system (due to longer fault times and potential combustion energy) a greater volume being is vaporized and turned into particles. The particles increase in number while becoming smaller in size following a non-linear fashion (i.e., if a particle size (i.e. diameter) is split in half in dimensional, it produces eight times as many particles. This leads to a cubic growth rate of particle numbers for the same volume. Each of these particles are hotter and

[2] Aluminum is often used as a fuel in solid rocket motors, due to its extreme energy production. The heat of formation of aluminum and oxygen is -1676.7 kJ/mol.

any that hit the ground that exceed the autoignition temperature will have an opportunity to create a fire. The particle count equation used here varies; in some instances, it assumes a squared term based on fault time, in others it is more linear.

Currently, the particle hazard equation is dependent only upon simple input variables – fault time and amperage. Each equation is specific to conductor type and fault configuration. The conductor type (397 MCM Al, #4 ACSR, or 3/0 Cu) is a purely qualitative measure, and further work based on the physics associated with each material (specific heat, thermal conductivity, density, melting and vaporization temperatures, and in the case of aluminum, including combustion energy) would be necessary to clarify a complicated physical relationship. However, further evolution of the hazard equation can incorporate wind speed into the equation in order to assess particle spread.

Parallel and Pigtail configurations result in specifically different particle production for the same material, likely due to the focus point of the Pigtail as opposed to the rapidly changing arcing point associated with Parallel lines. The two conditions introduce further uncertainty that may not be possible to exactly quantify. However, Pigtail configurations produce in almost all cases an order of magnitude or greater particles. The Pigtail Configuration is responsible for more fires as well; for the Lift tests, 73% of all Pigtail tests for the three major conductor types produced a fire. The Parallel Configuration was responsible for 22% of all fires for that configuration. No fires were observed for 397 MCM Al Parallel configuration for either the Cage or Lift tests.

Specifically, in the “Lift” components of the testing, when particle temperatures were not greater than paper ignition temperature, there were no fires observed. The Lift tests were most representative of what might occur in the field, and therefore were of greater import for this analysis. Of critical importance here was that in almost all instances, low particle production and lower particle temperatures were associated with the smallest fault interrupt times (0.1 seconds, 0.25 seconds) and a correspondingly reduced chance of resultant fires (as seen in the Lift tests). Higher particle counts and higher counts of high temperature particles were strongly associated with longer fault interrupt times (0.5 seconds, 1.0 seconds) and resultant fires (again, as seen in the Lift tests).

Of further note, the number of total particles rose at a non-linear rate. We hypothesize that these were smaller, hotter particles, with the second part of this borne out by the counts of particles that exceeded autoignition temperature of paper (greater than 210 °C). Particle counts increased at least at a rate that was based on a squared function, if not greater, by fault interrupt time; this also points to the importance of attempting to reduce fault interrupt times as much as possible in order to reduce fire risk. It is believed that this rapid, non-linear increase is due to smaller particle production (with particle size decreasing and increasing particle size by cubic rates).

One major takeaway is that hazardous particle production does not rise linearly in all cased as fault time increases. Since interrupt times do not have a linear impact on particle production, faster interrupt times significantly impact fire safety, especially for aluminum and ACSR conductors. Particle hazard as a function of the square of current and fault time, although copper shows a more linear rise than the aluminum type conductors. This was a surprising result of the tests, one that could help develop better procedures to minimize fire risk from particle production by reducing fault time. Another usage of the particle hazard equation could be to assess proper brush clearances.

7 REFERENCES

Graf, S.H., 1949. Ignition temperatures of various papers, woods, and fabrics. Bulletin No. 26, March 1949. Engineering Experiment Station, Oregon State University, Corvallis, OR.

Jacobson, M., Cooper, A.R. and Nagy, J., 1964. Explosibility of metal powders (Vol. 6516). US Department of the Interior, Bureau of Mines.

Mills, A.F., 1984. Trajectories of sparks from arcing aluminum power cables. Fire Technology, 20(2), pp.5-14.

Mills, A.F., 1995. Heat and mass transfer, Richard D. Irwin, Boston.

Trunov, M.A., Schoenitz, M. and Dreizin, E.L., 2005. Ignition of aluminum powders under different experimental conditions. Propellants, Explosives, Pyrotechnics: An International Journal Dealing with Scientific and Technological Aspects of Energetic Materials, 30(1), pp.36-43.

Wilson, W.R., 1955. High-current arc erosion of electric contact materials [includes discussion]. Transactions of the American Institute of Electrical Engineers. Part III: Power Apparatus and Systems, 74(3), pp.657-664.